

Spark Model for Pulsar Radiation Modulation Patterns

J.A. Gil, M. Sendyk

J. Kepler Astronomical Center, Pedagogical University, Lubuska 2, 65-265, Zielona Gora, Poland

jag@astro.ca.wsp.zgora.pl

ABSTRACT

A non-stationary polar gap model first proposed by Ruderman & Sutherland (1975) is modified and applied to spark-associated pulsar emission at radio wavelengths. It is argued that under physical and geometrical conditions prevailing above pulsar polar cap, highly non-stationary spark discharges do not occur at random positions. Instead, sparks should tend to operate in well determined preferred regions. At any instant the polar cap is populated as densely as possible with a number of two-dimensional sparks with a characteristic dimension as well as a typical distance between adjacent sparks being about the polar gap height. Our model differs, however, markedly from its original "hollow cone" version. The key feature is the quasi-central spark driven by γ - γ pair production process and anchored to the local pole of a sunspot-like surface magnetic field. This fixed spark prevents the motion of other sparks towards the pole, restricting it to slow circumferential $E \times B$ drift across the planes of field lines converging at the local pole. We argue that the polar spark constitutes the core pulsar emission, and that the annular rings of drifting sparks contribute to conal components of the pulsar beam. We found that the number of nested cones in the beam of typical pulsar should not exceed three; a number also found by Mitra & Deshpande (1999) using a completely different analysis. We confront predictions of our model with a variety of pulsar data, including mean profile morphology and their predicted correlations with properties of the P–P–pulsar diagram as well as detailed studies of drifting subpulses (Deshpande & Rankin 1999). We demonstrate that, if the observing geometry is known, the average profile as well as the apparent drift pattern are fully determined by the values of P and \dot{P} . In the accompanying Paper II we develop a self-consistent theory of coherent pulsar radio emission based on the modified polar gap model explored in this paper.

Subject headings: pulsars: general { radio emission { drifting subpulses { mean profiles

1. Introduction

Pulsar radiation is believed to originate within a bundle of open magnetic field lines, along which a significant part of a rotation induced potential drop can occur. This potential drop accelerates charged particles supplied by the polar cap area, which is a region of the neutron star

surface directly connected to the interstellar medium via magnetic field lines. Two types of polar cap activity models have been proposed so far. In the first type, called the free-flow or stationary models (Sharlemán et al. 1978; Arons & Sharlemán 1979; Arons 1981), the charged particles flow freely from the polar cap surface and accelerate within a scale height of about one stellar radius $R \sim 10^6$ cm, due to the potential drop resulting from the curvature of field lines and/or inertia of outstreaming particles. In the second type, called gap models or non-stationary models (Sturrock 1971; Ruderman & Sutherland 1975 – RS75 henceforth; Cheng & Ruderman 1977, 1980), the free outflow from the polar cap surface is strongly impeded, which leads to the formation of an empty gap just above the polar cap. The high potential drop across the gap is discharged by the photon-induced pair creation in the strong and curved magnetic field. This breakdown of the polar gap stabilizes its height to about one mean free path for the $E \sim B$ pair production process, which has to be smaller than the polar cap radius $r_p \sim 10^4 P^{1/2}$ cm, where P is pulsar period in seconds. The charges of opposite signs are accelerated in opposite directions to energies exceeding $2m_e c^2$ and a cascade avalanche develops. The polar gap breaks in the form of a number of isolated, short-lived discharge tubes called sparks (Cheng & Ruderman 1977; Beskin 1982; Filippenko & Radhakrishnan 1982), which can be naturally interpreted in terms of subpulse-associated plasma columns, modulating the pulsar radiation spatially on the subpulse time-scales (~ 1 ms).

The plan of the rest of this paper follows. In section 2 we revise the RS75 model in such a way that it is no longer the hollow cone type model. We assume that the surface magnetic field is non-dipolar, with a typical radius of curvature much smaller than the neutron star radius $R < 10^6$ cm (Blanford et al. 1983; Romani 1990; Ruderman 1991; Krolik 1991; Arons 1993; Chen & Ruderman 1993; Mitra et al. 1999). We also assume that the planes of the magnetic field lines should tend to converge at the local pole, introducing some degree of axial symmetry like in the case of "sunspot" field configurations (Chen & Ruderman 1993; Gil & Mitra 1999, see also Appendix). We follow the RS75 idea that the high potential drop above the polar cap is discharged via a number of localized spark elements and argue that one of them should be anchored to the local surface pole, while others should perform more or less ordered circumferential motion around it due to the well-known $E \sim B$ drift. However, we take into account reduction of the vacuum accelerating potential drop (eq. [2]) due to spark development (eq. [4]), which reduces also the apparent drift rate (eqs. [10], [14] and [13]). We argue that both the characteristic dimension as well as the typical distance between sparks should be about the RS75 gap height (eq. [1]). We use this result in section 3, where we propose that polar spark is associated with the core pulsar emission, while concentric rings formed by drifting sparks correspond to nested conal components of the "non-hollow cone" radiation pattern. We calculate the number of cones in the pulsar beam and, since it depends mainly on the values of basic pulsar parameters P and P_{-} , we examine correlations of number of profile components and profile types with properties of standard P – P_{-} diagram. The degree of correlations is high, supporting our picture. In section 4 we revise the RS75 subpulse drift model and apply it to a number of pulsars with drifting subpulses. In section 5 we incorporate the behaviours of drifting subpulses into the core/cone morphological model of pulsar proposed and developed by Rankin (1983). We discuss both general and specific implications of our model in

section 6. In the Appendix we briefly discuss evidence of nondipolar surface magnetic field from PSR J2144-3933, the recently reported 8.5-s pulsar.

Despite a number of well-known problems with the neutron star crust binding energy (see Xu et al. 1999, for short review), the recent papers concerning pulsars with drifting subpulses PSR 0943+10 (Deshpande & Rankin 1999) and PSR 0031-07 (Vivekanand & Joshi 1999) strongly suggest that the RS75-type vacuum gap does exist above the polar cap. Motivated by these evidences, Xu et al. (1999) have recently argued that the binding energy problem can be completely solved if pulsars (at least those with drifting subpulses) represent bare strange stars, which in many aspects are indistinguishable from neutron stars.

Sparks proposed in the RS75 model as primary sources of the subpulse-associated plasma columns have been criticized, mainly due to short dynamical time scales ($\sim 10^{-10}$ s) as compared with subpulse time scales (~ 1 ms). To account for the subpulse emission, they would have to repeat at approximately the same place for a time long relative to their lifetime. No clear explanation for such kind of a surface memory was proposed by RS75. In this paper we propose a modification of the RS75 polar gap model and confront the predictions of the revised model with the much larger body of present day observational data, concerning both subpulses in single pulses and average profiles.

New ingredients of our modified RS75 model include: (a) estimation of a characteristic spark dimension D_{spark} (eqs. [1] and [9]), (b) introduction of quasi-central spark anchored to the local pole of surface magnetic pole (thus our model is no longer of a hollow-cone type); (c) reduction of gap potential drop corresponding to subpulse emission by a filling factor $F < 1$ (eq. [4]). The critical assumption we need to adopt is an existence of a local magnetic pole (different from the global dipole) at the polar cap. This is necessary for two reasons: (i) a radius of curvature of surface magnetic field is small enough to drive and exponentiate spark discharges in the first place; (ii) the spark fixed at the local pole warrants a persistence of spark arrangement in the form of a quasi-annular pattern leading to nested cone structure of the pulsar beam. Such a multiconal organisation of pulsar beams was first suggested by Rankin (1983, 1993a, b), supported by Gil et al. (1993) and confirmed ultimately by Mitra & Deshpande (1999). The recently reported pulsar with longest period $P = 8.5$ s (Young et al. 1999) suggests that the surface magnetic field in pulsars has a sunspot-like configuration (Chen & Ruderman 1993; Gil & Mitra 1999, see also Appendix). We argue that one of the local poles is located at the Goldreich & Julian (1969) polar cap, and assume that pulsar radio emission originates on those multipolar surface field lines which reconnect with dipolar ones in the radio emission region.

2. Polar gap sparking discharge

In this section we discuss the spark reappearance and spark characteristic dimension problems. As described by RS75, the polar gap discharges through a number of localized sparks, separated

from each other by a distance approximately equal to the gap height

$$h = 5 \cdot 10^{12} B_{12}^{4/7} R_6^{2/7} P^{3/7} \text{ cm}; \quad (1)$$

where P is pulsar period in seconds, $B_{12} = B_s/10^{12}$ G is the surface magnetic field in units 10^{12} Gauss and $R_6 = R/10^6$ cm is the radius of curvature of surface field in units of $R = 10^6$ cm. We assume that surface magnetic field B_s is highly multipolar, that is $B_s = b B_d$, where $B_d = 3.2 \cdot 10^8 (P/P_0)^{-1/2}$ G and a dimensionless factor $b \sim 1$. It seems natural to assume the range of dimensionless curvature radii from within the range $0.1 < R_6 < 1.0$ (Gil & Mitra 1999, see Appendix). Each spark develops exponentially until the plasma density reaches a value close to the corotational Goldreich-Julian (1969) density n_{GJ} , screening the gap locally. The potential drop within the spark filament is roughly $V = (1 - \alpha_{GJ}) V_{max}$, where $\alpha < \alpha_{GJ}$ and the maximum RS75 potential drop

$$V_{max} = 1.7 \cdot 10^6 R_6^{4/7} B_{12}^{1/7} P^{-1/7} V; \quad (2)$$

The spark exponentiation stops abruptly when α approaches α_{GJ} . The potential drop V is reduced to a value slightly below the threshold for B pair production

$$V_{min} = m_{in} m_e c^2/e; \quad (3)$$

where

$$m_{in} = (2m_e c^2 R / \hbar c)^{1/3} \sim 3.3 R_6^{1/3} 10^5;$$

In this expression \hbar is the Planck constant, e and m_e is the electron charge and mass, respectively, and c is the speed of light. Note that unlike equation (2), equations (3) and (4) represent a necessary but not sufficient condition for magnetic pair production within the polar gap. One can therefore introduce a filling factor

$$F = \frac{V_{min}}{V_{max}} \sim 0.1 R_6^{5/21} B_{12}^{1/7} P^{1/7} \sim 1; \quad (4)$$

which determines a saturation stage at which the spark plasma begins to leave the gap. We will call it the "gap emptying stage", in which spark plasma is dense enough to contribute efficiently to the mechanism of generation of coherent radio emission (see Paper II). When the spark plasma leaves the gap with a speed $v < c$, the potential drop beneath the spark rapidly grows and it should exceed the threshold value for B pair creation before the bottom of the spark filament reaches the top of the gap. It is obvious that the gap emptying stage does not begin simultaneously in adjacent sparks, each screening the area within a distance $h \sim 5 \cdot 10^{13}$ cm. Therefore, the returning potential drop will be larger beneath the leaving spark plasma than around it and the very next cascade should be initiated and developed in approximately the same place as the previous one, provided that the spark plasma does not move fast in any direction during the exponentiation time. Such motions are prevented by a putative spark anchored to the local pole. This will be discussed in more detail later in the paper.

In order to avoid confusion, we will now give a short summary of the remaining part of this section, so the reader knows what to expect. First we estimate a characteristic spark dimension D_{\perp} as seen by observer's line-of-sight (perpendicular to the planes of field lines converging at the local surface pole). Next, we estimate a characteristic dimension D_k resulting from a rapid spread of spark avalanche within the planes of field lines (parallel). Then we notice that since $D_k \gg D_{\perp} \gg h$, a mechanism must exist broadening an avalanche also in the perpendicular direction. We invoke a photon splash known from literature. All in all we argue that sparks should be a two dimensional entities on the polar cap, with a characteristic dimension $D \approx D_{\perp} \approx D_k$, as well as a separation of adjacent sparks, being about the polar gap height $h \approx 5 \cdot 10^{3-7}$ cm in typical pulsars.

Interpreting the width of subpulses as radio emission from plasma columns flowing along dipolar field lines connected to sparks, one can estimate the fraction $(D/r_p^d)^2$ of the polar cap area filled by a spark being in the range 10^{-1} to 10^{-2} (Cheng & Ruderman 1977), where D is a characteristic spark dimension referred to a dipolar polar cap. We can form a dimensionless parameter

$$r_p^d = h_{RS} = 5 \cdot 10^6 P^{2=7} P^{-9=14} ; \quad (5)$$

where $r_p^d = 10^4 P^{-1=2}$ cm is the Goldreich-Julian (1969) polar cap radius and $h_{RS} = h$ (eq. [1]) is the RS75 polar gap height with a dipolar component of surface magnetic field $B_{12} = B_{12}^d$ (in units of 10^{12} Gauss). For a typical pulsar with $P = 1$ s, $\dot{P} = 10^{-15}$ and $R_6^{2=7} = 0.7$ this equation gives $h_{RS} \approx 0.2 r_p^d = 2 \cdot 10^6$ cm. On the other hand $\langle D/r_p^d \rangle = \frac{P^{2=7}}{0.05} \approx 0.2$ or $D \approx 0.2 r_p^d$. By comparison one can conclude that $D \approx h_{RS}$. This means that the characteristic dimension of the subpulse-associated plasma column projected onto the polar cap along dipolar field lines is approximately equal to the RS75 polar gap height h (eq. [1]). One should emphasize, however, that this is only observational constraint corresponding to the dimension along the line-of-sight, as there is no direct information available about the other dimension. However, Deshpande & Rankin (1999) using their cartographic transform technique applied to good quality single pulse data of PSR 0943+10, clearly demonstrated that sparks are two-dimensional, approximately circular entities related to drifting subpulses, as originally proposed by RS75 (see also Fig. 1 in this paper for illustration).

In the case of the dipolar surface magnetic field D can be directly interpreted as a spark characteristic dimension (at least in the direction along the line-of-sight). In the actual pulsar however, both the polar cap radius and the polar gap height have to be modified to include higher multipoles dominating the global dipole magnetic field at the polar cap surface. As a result, equation (5) should be replaced by

$$r_p = h = b^{1=14} r_p^d = h_{RS} ; \quad (6)$$

where $r_p = b^{1=2} r_p^d$ and $B_{12} = b B_{12}^d$. As one can see, the actual ratio $r_p = h$ does not differ by more than a factor of two from the canonical value (eq. [5]), even if the actual surface magnetic field is 10^4 times stronger than the dipolar component inferred from the pulsar slow down rate. This simply means that the angular ratio of the spark-associated plasma column to the open field

lines region is preserved down to the polar cap, no matter how complicated the surface magnetic field is. Treating b as a constant in equation (6) means that we assume that the actual surface magnetic field evolves similarly to that of purely dipolar field. As demonstrated recently by Mitra et al. (1999), such assumption is quite well justified.

One can attempt to estimate the spark dimension using an independent argument. The number density of the e^-e^+ pairs in the sparking avalanche should develop exponentially with time. To estimate precisely the spark exponentiation time, that is the characteristic time-scale after which the spark charge density reaches the corotational value n_{GJ} which screens the gap (where n_{GJ} is the Goldreich-Julian (1969) number density), one would require a detailed physical model for pair formation and spark development within the gap region. So far such a model does not exist and we have to use arguments based on a general picture of pair creation in strong curved magnetic fields (Eriber 1964, RS75) and dimensional analysis. Let us notice that the exponentiation time-scale should be approximately proportional to the radius of curvature R of the surface magnetic field. In fact, copious magnetic pair production within the gap requires a large perpendicular component of the magnetic field $B_\perp = hB/R$. For a given h and B , the curvature photon has to travel a distance $l \approx h$ to reach a value of B_\perp high enough to produce a pair. The smaller the radius of curvature R , the smaller the distance l and, in consequence, the shorter the time-scale. Thus, a natural spark exponentiation time-scale is

$$R = c\tau \quad (7)$$

For a small radius of curvature $R \approx 10^8$ cm (see Appendix) this is about 10 ns, which is equal to the value obtained by independent arguments in the RS75 model (see also Beskin 1982 and Asseo & Melikidze 1998).

If the surface magnetic field is not extremely tangled and possesses some degree of quasi-axial symmetry, like in the case of sunspot-like configuration, the sparks will develop (at least initially) in the form of thin plane sheets, following the planes of field lines converging at the local pole. In fact, the spark plasma is subject to fast parallel drift motion towards a local pole (in the direction opposite to field lines curvature) with a speed

$$v_k = c h/R \quad (8)$$

(Cheng & Ruderman 1977, 1980; Filippenko & Radhakrishnan 1982). Thus, during the exponentiation time $\tau = R/c$ the spark will cover a distance $D_k = v_k \tau = h$ (hc/R) ($R=c$) = h . This can also be considered as a characteristic spark dimension (in the planes of field lines converging towards a local magnetic pole). As one can see, D_k is equal to the perpendicular spark dimension D_\perp inferred from the subpulse widths analysis. Therefore, a mechanism has to exist which spreads an initially thin and plane discharge into a two-dimensional entity with a characteristic dimension

$$D \approx h; \quad (9)$$

where h is the gap height (eq. [1]). One such mechanism, called a "photon splash" effect has been proposed by Cheng & Ruderman (1977). It occurs when a very energetic electron (positron) impacts

the pulsar surface. As a result, at least one secondary high-energy ($> 1 \text{ MeV}$) gamma ray is emitted. Since this emission is unidirectional, the photon splash can effectively blow a spark virtually in all directions within the limit of a free path for e^+e^- pair production, which is approximately equal to the RS75 gap height h . Thus, a fully developed spark should be approximately circular in shape with diameter $D \approx h$ (eq. [9]), as demonstrated recently by Deshpande & Rankin (1999) analyzing the case of drifting subpulses in PSR 0943+10 (see also Fig. 1 in this paper).

In principle, the spark plasma is subject to two drift motions: fast "parallel" drift along the planes of field lines with a velocity described by equation (8) and a much slower "perpendicular" $E \times B$ drift (RS75) across the planes of field lines with a velocity

$$v_\perp = c \frac{E}{B_s} = F \frac{2}{P} \frac{h^2}{r_p(1-s)}; \quad (10)$$

where $r_p = 10^4 P^{-1/2} \text{ cm}$ is the polar cap radius, $E = F(2 - \cos\theta) h^2 / r_p(1-s)$ is the gap electric field perpendicular to the surface magnetic field B_s , F is the filling factor corresponding to the spark termination stage (eq. [4]) and $s = d/r_p$ is the mapping parameter ($0 < s < 1$) of field lines associated with a spark operating at a distance d from the pole. Typically $v_k \approx v_\perp$, so $E \times B$ drift is not expected to influence the spark shape. It will however, cause the slow motion of fully developed sparks around the local centre of axial symmetry, determined by the pole of sunspot-like surface magnetic field.

Let us consider an avalanche discharge which by chance occurred close to the local pole of the multipolar surface magnetic field (which is quite likely to happen given a large number of energetic -quanta penetrating the gap region; see RS75). Due to both parallel and perpendicular drift motions as well as a putative quasi-axial symmetry at the pole, this discharge will very soon anchor itself to the polar area and form a fixed spark ($E \times B$ circulating around "itself"). This should happen independently of any details of polar gap discharge. In fact, at the very beginning sparks will rush towards the local pole due to quasi-axial symmetry of field line planes. Once a spark reaches a pole it begins to circulate around itself (due to $E \times B$ drift). We will interpret this fixed polar spark as the source of plasma column related to the core pulsar emission (Rankin 1983, 1990). Other sparks, which can form at a screening distance $h \approx h_S$ from the polar spark and from each other (see Fig. 1 for illustration), will perform circumferential $E \times B$ drift around the pole. It is natural to interpret plasma columns associated with these sparks as sources of the conal pulsar emission (Rankin 1983, 1990, 1993a, b).

To summarize this section; when a sparking discharge begins at some point on the polar cap, the gap potential drop rapidly falls below the e^+e^- pair formation threshold, which should inhibit another discharge within a distance of about h (eq. [1]). The fixed polar spark thus restricts degrees of freedom of other sparks to circumferential motion around the pole, as they cannot approach the polar one within a screening distance h . The existence of the polar spark is therefore crucial for our model. Within the e^+e^- pair production mechanism of gap discharge, it requires that the polar field lines are sufficiently curved (like in a "sunspot" configuration). However, one cannot exclude

that the actual gap magnetic field is fully axially-symmetric (like the case of a star-centered dipole or quadrupole). In such a case the polar field lines are not curved enough to maintain a cascade of π B pair production. Zhang & Qiao (1998) have recently proposed an alternative two-photon pair production process, which may perhaps account for the formation of a polar spark in a fully symmetric field configuration, in which there is not enough curvature to drive pair production at the pole.

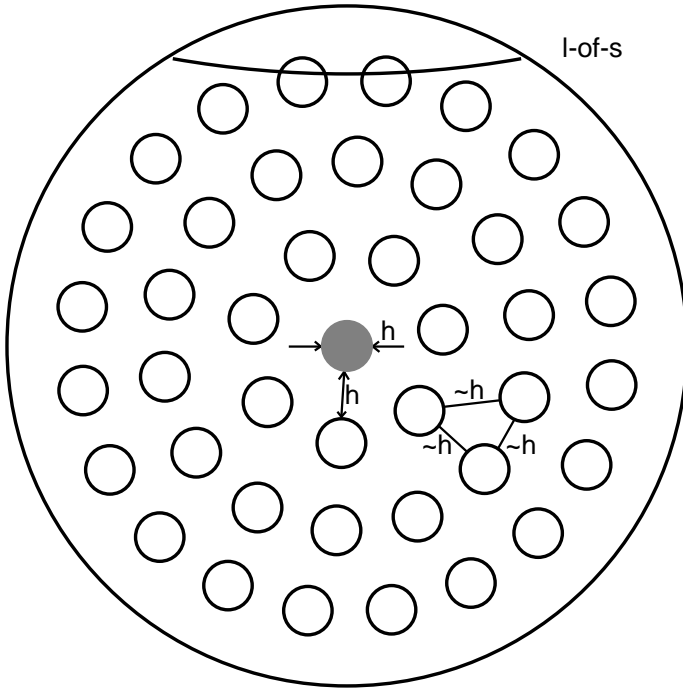


Fig. 1. The illustration of instantaneous arrangement of a number of equidistant sparks on the polar cap of PSR B0943+10. The shadowed spark is anchored to the local pole of the surface magnetic pole while other sparks perform a slow $E \times B$ drift around it. The line-of-sight cuts through the outermost ring of 20 equally spaced sparks at the impact angle $\theta = 8^\circ$ from the pole (for comparison see the map of 20 subpulse beams in Deshpande and Rankin, 1999). Both the HPBW of each spark and a distance between adjacent sparks is about $h = r_p a \approx 17$ m, where the polar cap radius r_p is about 110 m and the complexity parameter $a \approx 6.5$ (see section 4.1 for explanations).

3. Polar cap structure and mean pulsar beams

As argued in previous section, the actual pulsar polar cap should be populated by a number of sparks with a characteristic dimension $D \approx h$, separated from each other also by about h , where h is

the actual gap height close to the value given by RS75 (eq. [1]). One spark should be always active at the local surface magnetic pole, and other sparks should perform more or less ordered, circular $E \times B$ drift motion around the polar spark. In this sense our model differs markedly from the RS75 hollow-cone version in which sparks occupied only an outermost parts of the polar cap. Since the polar spark prevents the motion of other sparks towards the pole, the drifting sparks should form on the average a multi-ring structure centered on the polar spark. These rings are not expected to be perfectly circular, as we assume only quasi-axial symmetry of field line planes converging at the pole of a surface magnetic field. It is natural to assume that plasma supplied by sparks to the magnetosphere above the polar gap will eventually give rise to the subpulse emission (see Paper II) at altitudes of a few percent of the light-cylinder radius $R_{LC} = cP/2$ (Cordes 1992, Kijak & Gil 1997, 1998). The subpulses associated with the polar spark should be longitude-stationary and constitute the so called "core component" in the mean pulsar profile, while other subpulses may demonstrate an organized drift from one pulse to another and contribute to the so called "conal components" in the mean pulsar profile. In section 5 we discuss distinction between core and conal profile components in more detail.

We would like to emphasize that the ring structure of the polar cap mean energy distribution is a consequence of (i) fixed spark at the local pole, and (ii) screening distance between adjacent sparks approximately equal to spark dimension (Fig. 1). This structure will result in a specific organization of the mean pulsar emission pattern, consisting of a narrow core beam surrounded by a number of nested conal beams. Simulations of pulsar emission within the framework of the above model seem to reproduce the observational properties of both single pulses and mean profiles quite well (Gil et al. 1995, Gil & Kravczyk 1996, 1997). Such a nested cone structure of pulsar beams have been suggested by many authors (e.g Rankin 1993; Gil, Kijak & Seiradakis 1993; Kramer et al. 1994). Alternatively, the patchy beam model has also been proposed to explain variety of pulsar profiles (Lyne & Manchester 1988). However, as demonstrated by Gil & Kravczyk (1996), the patchy beam model is inconsistent with the observed frequency evolution of subpulses as contrasted with profile components. Also Mitra & Deshpande (1999) have recently presented strong arguments against patchy beams or even thick hollow cone beams. Analyzing multifrequency pulse-width data, Mitra & Deshpande clearly revealed a nested cone structure of pulsar beams and found that each cone is illuminated in the form of annular ring of width being typically about 20 percent of the overall beam radius (opening angle). This is in perfect agreement with our ratio of spark diameter to polar cap radius $D = r_p \approx 0.2$ (see discussion below equation (5)).

Within our geometrical model of the polar cap, the complexity of pulsar emission pattern should just be determined by this ratio of the polar cap radius $r_p \approx 10^4 P^{1/2}$ cm to the spark characteristic dimension $D = h \approx 5 \cdot 10^{-2} P^{2/7} P^{1/7}$ cm. Following equations (5) and (6) we will introduce a complexity parameter

$$a = \frac{r_p}{h} \approx 5 P_{-15}^{2/7} P^{9/14}; \quad (11)$$

where $P_{-15} = P/10^{-15}$. To make it possibly independent of unknown characteristics of the actual

$$\{ 10 \{$$

surface magnetic field, we have assumed that $b^{14} R_6^{2=7} \approx 2$ (which is roughly the case for all realistic combinations of $b > 1$ and $R_6 < 1$; see Appendix).

Each spark can be modelled with a Gaussian of half-power beam width about h . According to RS75, distance between HPBW points is also about h . This means that the complexity parameter a (eq. [11]) determines roughly a number of equi-spaced sparks $N_{sp} \approx a^2$ (see Fig. 1 for illustration) that can operate on the entire polar cap at any given time (see also Beskin 1992). It is natural to assume that these sparks, rotating around fixed spark anchored to the local pole, form on the average a system of nested cones in the pulsar beam. We additionally assume that the fixed spark contributes to the core pulsar emission. The number of nested cones surrounding the core beam can be roughly described by

$$n = \text{Int} \left(\frac{a}{2} \right) : \quad (12)$$

(half of the Gaussian sparks that can be fit along a polar cap diameter, excluding the one fixed at the pole). As a consequence of equations (11) and (12), the number of components resolved in the average pulsar profile is approximately given by

$$N = N_{max} = 2n + 1 = \text{Int}(a); \quad (13)$$

depending on the observer's impact angle, where the equality holds when the light-of-sight passes close to the axis associated with the core beam. However, it should be stressed that profile components can be resolved only for relatively small values of the complexity parameter $a < 10$ (for $a > 10$ the above equation reads $N = 1$; see section 5.3b).

The subpulse emission in single pulses can be resolved only if the value of a is not too large. This means that subpulses (possibly drifting) can be detected in pulsars with relatively small values of a , which occurs in older pulsars. The radio emission of younger pulsars with shorter periods should be predominantly amorphous with no hints of modulation on the subpulse time scales.

4. Spark-associated subpulse drift

The E-B drift across the planes of field lines converging at the local pole, responsible for creating a nested cone structure of average pulsar beams, should manifest itself as a prominent subpulse drift and/or periodic intensity modulation in subpulses associated with conal components. The thick circles in Fig. 5 indicate presence of drifting subpulses in single pulses of corresponding pulsars. As demonstrated by Rankin (1986) drifting subpulses are a purely conal phenomenon. It is clear from our model why drifting subpulses tend to occur mostly in conal components of complex profile pulsars (M; Q; cT; D; S_{cl}) and never in core-single (S_t) profile pulsars. First, subpulses in core components of complex profiles cannot drift, since the corresponding spark is anchored to the local magnetic pole. As for the core-single pulsars (S_t), the lack of an apparent subpulse drift is a consequence of unresolved subpulse beams in their pattern emission (see section 5.3 for

explanation). However, subpulse drift is in principle possible in the conal outriders developed at higher frequencies and in conal components of Triple (T) profile pulsars (Rankin 1983).

The E-B drift results in a slow circumferential motion of sparks around the local pole of surface magnetic field. The spark associated plasma column completes one rotation in a time interval

$$\hat{P}_3 = 2\pi d/v_\varphi = (P/F) \frac{2\pi a}{s(1-s)}; \quad (14)$$

where $d = s_p r_p$ is distance of spark centre from the pole (the mapping parameter $s = 0$ at the pole and $s = 1$ at the polar cap edge $d = r_p$), v_φ is the speed of circulation described by equation (10) and $a = r_p h$ is the complexity parameter (eq. [11]). The number of circulating sparks which contribute to the observed drift pattern is

$$N = \hat{P}_3 = P_3; \quad (15)$$

where P_3 is the number of periods P between two primary drift-bands. The rate of circulation is $D = 360 \hat{P}_3$, which for typical pulsars is about 10 degrees per period. Let us note that if $n > 1$ (eq. [12]) then $N < N_{sp} \frac{1}{n^2}$.

The above equations represent modification of RS75 drift description in two aspects, namely: (i) they can be applied to spark at any distance $d = s_p r_p$ from the pole ($s = 0.5$ in RS75), provided that spark diameter $D \ll h_p d$, and (ii) the gap electric field is reduced by a factor $F < 1$ (eq. [4]) related to fully developed spark plasma ($F = 1$ in RS75). Below we explore the modified RS75 spark model in order to explain and reproduce patterns of drifting subpulses in a number of pulsars, for which good quality single pulse data were available.

Let us begin with a short summary. We will simulate the single pulse emission patterns of four pulsars by performing a number of subsequent steps: (i) determination of a number of nested cones and a number of sparks associated with the outermost cone (eqs. [11] and [12]); (ii) estimation of the mapping parameter s corresponding to the locus of the outermost cone; (iii) estimation of the approximate values of the inclination and impact angles using spectral and polarization information; (iv) determination of the fundamental periodicity \hat{P}_3 using equation (14); (v) estimation of emission altitude; (vi) calculations of the single pulse sequence corresponding to a system of drifting sparks (e.g. Fig. 1); (vii) matching the calculated and observed patterns by fine tuning the values of α and β , and if possible, testing the self-consistency of the model by calculating the expected polarization position angle curve and comparing it with that observed. For details of the simulation technique, see Gil et al. (1995).

4.1. PSR B 0943+10

Recently, Deshpande & Rankin (1999) have analysed in unprecedented detail an extraordinarily stable drifting-subpulse pattern of PSR B 0943+10 (see Fig. 2b). This is an interesting pulsar which exhibits the so-called even-odd modulation caused by the fast subpulse drift corresponding to the

apparent periodicity $P_3 = P/2$ (Sieber & Ooster 1975). This even-odd modulation manifests itself by apparent secondary driftbands of subpulses corresponding to every other pulse period. Of course, the primary driftbands corresponding to consecutive pulse periods are not visible in this pulsar. Deshpande & Rankin (1999) determined the observing geometry corresponding to a peripheral sightline grazing the outer beam, in which they were able to identify 20 rotating subbeam spots producing the apparent drift pattern. Each spark completes one full rotation in 37 periods P . Deshpande & Rankin (1999) have found this picture generally consistent with the system of sparks on the polar cap (RS75), with dimensions determined by the gap height. We provide a more specific description of the corresponding spark system, using equations (14) and (15).

The complexity parameter of this pulsar ($P = 1.098$ s; $P_{-15} = 3.52$) is 6.8 (eq. [11]). This implies that the mean radio emission should be arranged in $n = 3$ nested cones around the core beam (eq. [12]). The geometrical model of the polar cap for this pulsar shows 7, 14 and 20 spark-associated subpulse beams corresponding to 1st, 2nd and 3rd cone, respectively (Fig. 1). Given the grazing sightline geometry, an observer scans the outermost cone consisting of $N = 20$ subbeams circulating around the magnetic axis with a linear velocity determined by equation (10) and completing one full rotation in the time interval described by equation (14). The locus of the outermost cone on the polar cap corresponds to the mapping parameter $s_{\text{out}} = 0.875$. To obtain exactly the time interval $\hat{P}_3 = 37 P$ provided by the sophisticated analysis of Deshpande & Rankin (1999), we just need to adopt for a filling factor $F = 0.125$, which is perfectly consistent with $F \approx 0.1$ expected from equation (4). This value of F , together with $a^2 = 46$ and $s = 0.875$ gives $\hat{P}_3 = P = 36.8$ (eq. [14]). Let us note that according to equation (15) the apparent periodicity $P_3 = 1.85 P$, close to $P_3 = 1.89 P$ provided by Sieber & Ooster (1975).

It is worth to mention here that the "vacuum" value of \hat{P}_3 given by RS75 is much shorter (they use $F = 1$ and $s = 0.5$, for which values equation (14) gives $\hat{P}_3 = 11P$ if $N = 20$ and even less for $N < 20$). In fact, $\hat{P}_3 = P/5.6$ $\hat{P} = P^2$ in their model, which for $P = 1$ s and $B_{12} = 2$ gives $\hat{P}_3 = 9P$. Thus, the analysis of drifting subpulses in PSR B0943+10 performed by Deshpande & Rankin (1999) strongly supports our modified RS75 model.

To simulate single pulses of PSR B0943+10 at frequency 0.43 GHz (to be compared with the Arecibo data presented in Fig. 2b), let us consider a locus of the outermost cone containing 20 equi-spaced sparks at a distance $d = s_{\text{out}} r = 0.875 \times 110 \text{ m} \approx 100 \text{ m}$ from the magnetic pole. Both the HPBW diameter of sparks as well as distance between HPBW points is about $h = r_p a = 17 \text{ m}$. The line-of-sight grazes this cone in such a way that the observer can detect up to three spark-associated subpulses in a single pulse.

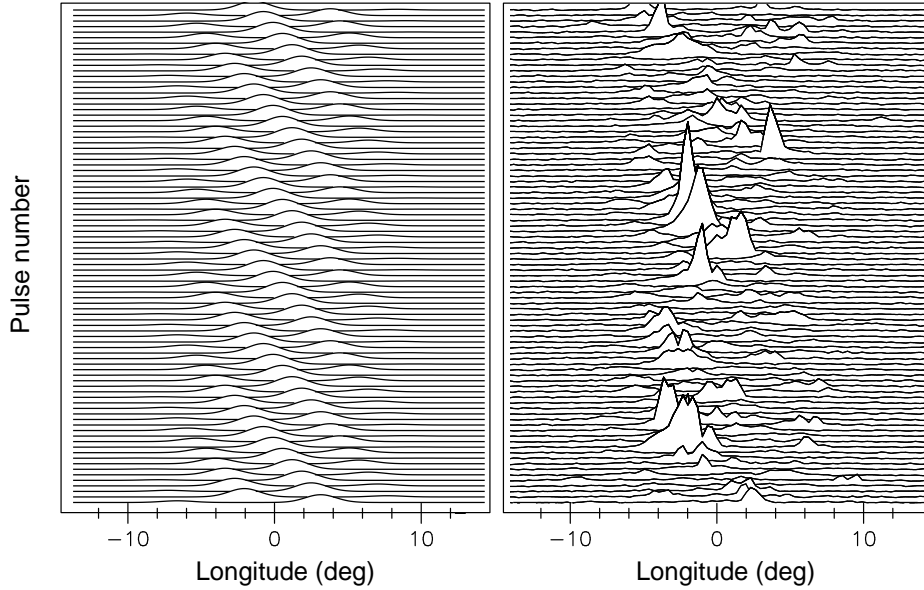


Fig. 2. | a. Simulated subpulse drift pattern for PSR B0943+10 (left-hand side) and | b. observed pattern (right-hand side) after Deshpande & Rankin (1999). The apparent secondary drift-bands consist of subpulses belonging to every other pulse period.

For $P = 1.1$ s and timing age $\tau_6 = 4.9$ million years we have emission altitude at 430 MHz $r_6 = r_{em} = R = 55 \frac{0.21}{\text{GHz}} \frac{0.1}{6} P^{0.33} = 60$ (Kijak and Gil 1997, 1998). Given the grazing sight-line geometry, we can reasonably assume that the opening angle of the beam of this pulsar at 430 MHz is about the impact angle. Thus $\sin \theta < (0.43) = 1.24 r_6^{1/2} (0.43)^{-1/2}$, which for $r_6 = 60$ gives $\sin \theta < 9$. On the other hand, from the polarization measurements we have $\sin \theta = \sin \theta = 3$ (Deshpande & Rankin 1999) and thus $\theta = \arcsin(3 \sin 9) = 28$.

Assuming $\theta = 28$ and $\theta = 9$ as initial values we will now perform calculations of the radiation emitted tangent to the dipolar field lines at altitude $r_{em} (0.43) = 60$ $R = 6 \cdot 10^6$ m, corresponding to a system of gaussian sparks presented in Fig. 1. Each spark circulates uniformly around the central polar spark (shadowed) at a rate of about 9.7 degrees per pulsar period ($360/37$). The resulting single pulse emission pattern is presented in Fig. 2a, in comparison with the 430 MHz observed pattern presented by Deshpande & Rankin (1999) in their Fig. 1, and reproduced here in Fig. 2b. We have obtained a "perfect match" by fine tuning geometrical parameters, which finally turned out to be $\theta = 26$ and $\theta = 8$. One can clearly see eight secondary drift bands corresponding to apparent even-odd modulation, which is exactly the sequence presented by Deshpande & Rankin (1999). The subpulses along secondary drift bands belong to every other pulse. The primary drift bands are not visible because subpulses drift very fast across the profile from one pulse to another. Less than two pulsar periods ($P_3 = 1.87 P = \text{cycle}$) are needed for the subpulse to reappear at the same longitudinal position, producing an apparent even-odd modulation

effect (secondary drift bands). This effect is so specific that it gives full solution (drift pattern and α ; values) in the simulation/fit procedure. Let us finally check for consistency that $N = \hat{P}_3 = P_3 = 37 = 1.85 \times 20$ (eqs. [14] and [15]).

4.2. PSR 2303+30

This is another pulsar showing precise intensity modulation along secondary drift-bands, formed from even and odd pulses separately. Individual pulses alternate between single-subpulse and double-subpulse form, with astonishing precision. The primary subpulse drift rate is so fast that subpulses drift across the pulse window from the edge of the pulse profile to its centre during about one pulsar period P . The apparent periodicity $P_3 = P$ is about 1.9 (Sieber & Ooster 1975). Our aim is to determine this fundamental periodicity \hat{P}_3 (eq. [14]) and the number of drifting sparks N (eq. [15]) forming the apparent secondary bands visible in Fig. 3b.

The high signal-to-noise ratio 430 MHz single pulse data have been recorded at the Arecibo observatory in August 1986 (Gil et al. 1992). A typical sequence of 150 single pulses of PSR B2303+30 is presented in Fig. 3b. One can distinguish two different types of phase-versus-intensity modulation in this sequence. Type A, visible near the top, demonstrates constant phase and intensity in both single and double pulses. Type A modulation is preceded and followed by Type B in which both phase and intensity of subpulses are modulated along secondary driftbands. The modulation is very precise with subpulse intensity strongly depending on its phase. The subpulses at the trailing edge are weak. The intensity gradually increases until it reaches a maximum near the center of the pulse window. Then it gradually decreases again toward the leading edge of the profile.

The single-pulse polarization characteristics of PSR 2303+30 are also very interesting. The position angle variation is presented in lower panel of Fig. 3b, which shows the position angle at the peak of subpulses (Gil et al. 1992). Filled symbols represent an intensity weighted average which can be interpreted as the Rotating Vector Model (RVM) curve (Radhakrishnan & Cooke 1969).

Thus, the intensity and polarization characteristics of PSR 2303+30 described above, are consistent with spark-associated subpulse beams rotating around the magnetic axis (see Gil et al. 1995 for discussion of polarization signatures of drifting subpulses). To simulate its emission, we note that the complexity parameter a (eq. [12]) in this case ($P = 1.57$ s; $P_{-15} = 2.9$) is about 5. This implies that there are two nested cones around the core beam ($a = 5$, $n = 2$; eqs. [12] and [11]) Geometrical model of such a polar cap shows that $s_{out} = 0.85$, with 12 sparks forming the outer cone. Since the apparent period $P_3 = 1.9$ (Sieber & Ooster 1975), thus according to equation (15), the circulation period (eq. [14]) $\hat{P}_3 = 23 \times P$, that is each spark completes one full rotation around the pole in about 23 periods $P = 1.57$ s. This corresponds to the circulation drift rate $D = 360/23 = 15.6$ per period P .

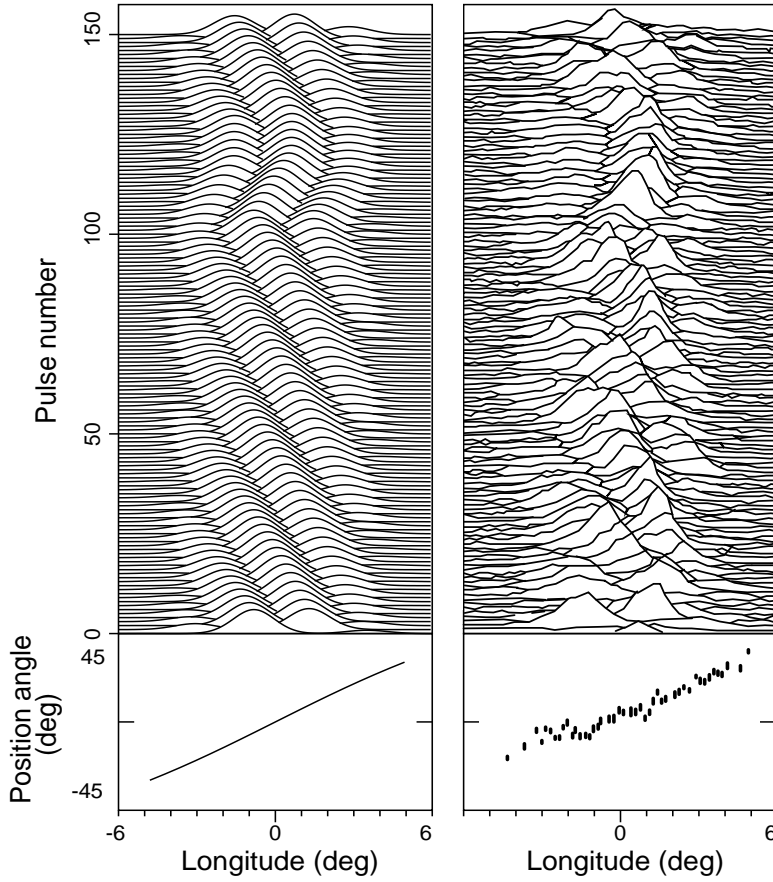


Fig. 3. | a. Simulated subpulse drift pattern for PSR B2303+30 (upper left-hand side) and | b. observed pattern (upper right-hand side) observed at 430 MHz from the Arecibo Observatory. Lower panels represent position angle variations: Rotating Vector Model for $\alpha = 50$ and $\beta = 6.7$ (left-hand side), and position angle values measured at subpulse peaks (right-hand side). Note that the apparent secondary drift-bands consist of subpulses belonging to every other pulse period.

We will now calculate the sequence of the first 100 single pulses of the type B, using the value of $D = 15.6P$ estimated above. The emission altitude at 430 MHz is $r_6(0.43) \approx 60$ with $\phi_6 = 8.63$ (Kijak and Gil 1997, 1998). We have found a number of secondary drift bands matching very well the observed pattern for $\alpha = 50$ and $\beta = 6.7$. These values can be used to estimate the position angle swing within the RVM model (Radhakrishnan & Cooke 1969). In fact, $\Delta\alpha = \alpha' - \alpha = \sin^{-1} \beta \sin \alpha = 6.5$, which gives 52 across ≈ 8.5 degrees of longitude occupied by the pulse window. This is exactly what is observed (compare lower panels of Figs. 3a and 3b), confirming again self-consistency of the model.

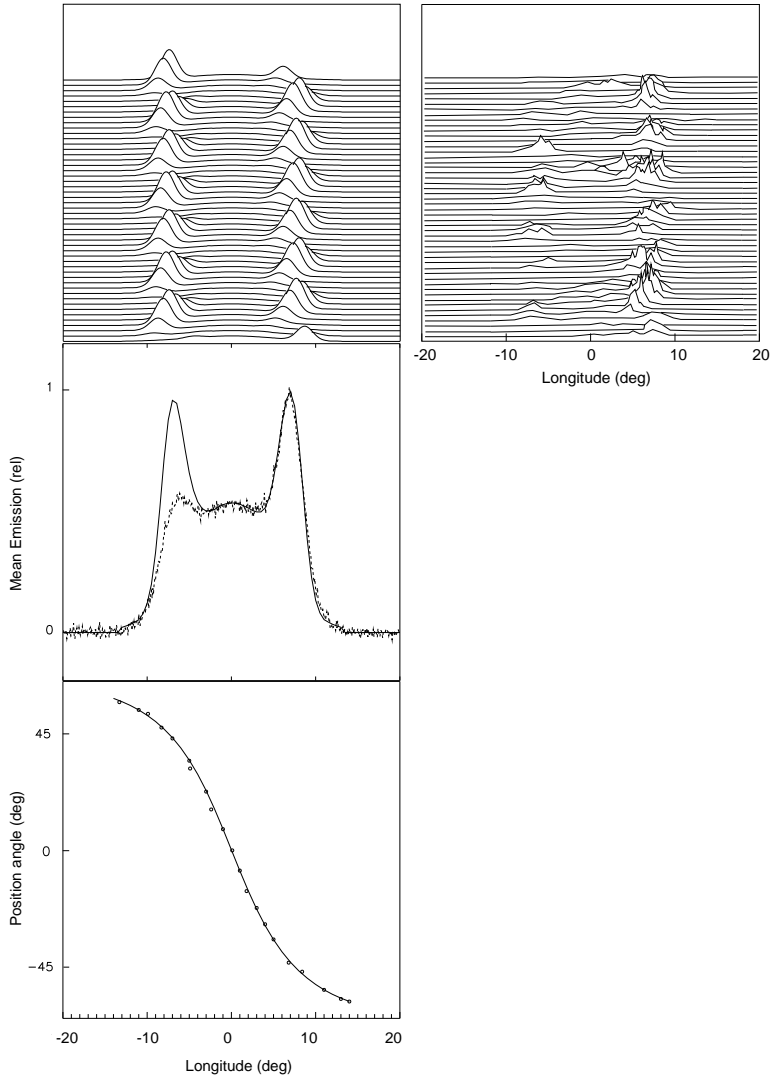


Fig. 4. | a Simulation of single pulses (left top panel), average profiles of both observational (dashed line) and simulated (solid line) data, and position angle variation (lower panel) of the observed data (circles) and model calculations (solid line) of PSR B2319+60. | b Sequence of 50 single pulses of PSR B2319+60 observed at 1.4 GHz in the Effelsberg Observatory (right panel), to be compared with simulated pulses in the left panel.

Above the pulse number 100, the secondary drift pattern changes into type A, first reversing a drift direction and then keeping a constant phase for about 20 periods. This corresponds to a slight change (less than 10%) in the circulation drift rate $D = 14:35=P$ and $14:97=P$, respectively, as compared with $15:6=P$ in the type B below and above. Since D/E (eqs. [10] and [14]), a dramatic change in the apparent secondary drift pattern from type B to type A corresponds to

only few percent change in gap electric field.

4.3. PSR 2319+60

This is another pulsar demonstrating a very specific pattern of drifting subpulses. The single pulse data at 1.4 GHz have been collected during the pulsar month (September 1991) at the Effelsberg Observatory (Fig. 4) and the average polarization data have been extracted from the Jodrell Bank database (Gould 1994). Since we have both a sequence of single pulse data and the average profile, we can obtain the values of the inclination and the impact angle in the procedure of fitting actual and simulated data. For $P = 2.26$ s and $P_{-15} = 7$ we obtain $a = 5.2$ and $n = 2$ (eqs. [11] and [12]). As before, the observed drifting subpulses belong to the second, outermost cone. The emission altitude at 1.4 GHz for $\ell_6 = 5$ is $r_6(1.4) = 57$ and $\ell_{out} = 5$ for $s_{out} = 0.85$. As one can see from Fig. 4, we reproduced quite precisely the sequence of drifting subpulses for $N = 9$ sparks. To match the observed primary drift rate $1:8=P$ we have to choose $F = 0.12$ (eq. [4]) and $\hat{P}_3 = 70P$ (eq. [14]). The simultaneous fit of single pulses and the average profile gives $\ell = 27$ and $\ell_3 = 3$. This implies the circulation rate $D = 6:2=P$. More importantly, the position angle curve calculated for these values of ℓ and ℓ_3 (solid line in Fig. 4) matches perfectly the observed values (dots), again confirming self-consistency of the model. Let us note that $P_3=P = \hat{P}_3/(N/P) = 7:8$, close to observed value (Fig. 4).

4.4. PSR B0031-07

Vivekanand & Joshi (1999) have recently published a sequence of drifting subpulses of PSR B0031-07, which we reproduce here in Fig. 5b. The authors report that the pair of drifting subpulses appears to be well separated and that their amplitudes are anti-correlated with each other. On rare occasions, three simultaneous subpulses seem to occur within one pulse. We demonstrate that this behaviour is quite natural and show the sequence of simulated single pulses (Fig. 5a) which match quite well the observed data (Fig. 5b).

Since for $P = 0.94$ s and $P_{-15} = 0.4$ the complexity parameter $a = 4$, the number of cones is either one or two (eqs. [12] and [11]). Let us examine the model with $n = 1$. The computer simulation gives $N = 5$ sparks at $s = 0.7$. Thus for $F = 0.1$, $\hat{P}_3 = 33.65/P$ and $3P/P = 34=5:6:8$ (eq. [13]), close to observed value (Fig. 5b). The model presented in Fig. 5a reproduces the observed sequence of drifting subpulses quite well (if one ignores the flux irregularities). In particular, one can see an anti-correlation of amplitudes and occasional three subpulses within one pulse. The calculations are related to frequency 327 MHz (Vivekanand & Joshi 1999), which implies the emission altitude $r_6 = r_{em} = R = 48$ (Kijak & Gil 1997, 1998). The observing geometry for one ring with five sparks gives $\ell = 13$ and $\ell_3 = 4.0$. The model with two rings requires 11 sparks on the outer ring, leading to $P_3 = \hat{P}_3/N = 34P/11 = 3P$, which is inconsistent with observations.

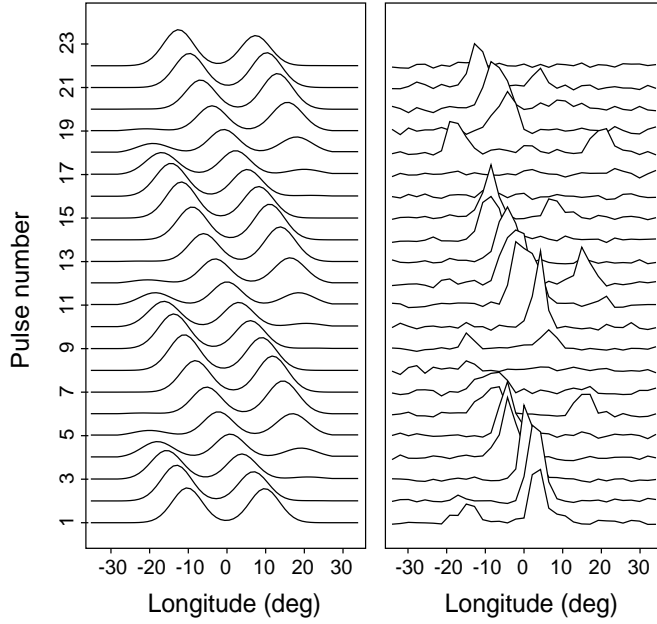


Fig. 5. | a. Simulated subpulse drift pattern for PSR B0031-07 (left-hand side) and | b. observed pattern (right-hand side) after Vivekanand & Joshi (1999). Note an occasional three subpulses within one pulse.

5. Profile classification and P-P diagram

Using equations (5), (6) and (11) we can calculate the period derivative (in units of 10^{-15} s/s)

$$P_{-15} = 3 \cdot 10^3 R_6^3 a^{3.5} P^{2.25}; \quad (16)$$

where the value of the complexity parameter $a = \frac{p}{p_h}$ can be obtained from the observed number of profile components (eq. [13]) or more precisely from Rankin's profile classification scheme (see below) and from the assumed range of $R_6 = 0.1$ (see Appendix). Figure 6 presents the P-P diagram for 539 pulsars, out of which is 182 classified within Rankin's scheme. For typical pulsars we follow classification established by Rankin (1983, 1986, 1990, 1993a, b) except profile types determined after 1993 in which case we follow Gould (1994). For millisecond pulsars we use Manchester & Johnston (1995), Xilouris & Kramer (1996), Kramer et al. (1998) and Xilouris et al. (1998).

For 182 classified pulsars, the value of the complexity parameter a is calculated from the equation (11) and represented in Fig. 6 by circle of different size (and colour corresponding to profile type). We excluded, for clarity of presentation, the three youngest pulsars with $a > 100$, so $1 < a < 100$ in Fig. 6. It is interesting that no pulsar with $a < 1$ exists. This means that we

can observe only those pulsars in which a mean free path for $\gamma\gamma$ pair production is shorter than the size of the polar cap ($h < r_p$). Another interesting fact is that the lines of constant complexity parameter a seem to follow a slope of 2.25, as can be expected from equation (16).

Rankin (1983, 1986) first proposed that the mean pulsar beam is arranged into a core beam surrounded by two conal beams. Her proposal was based on a careful analysis of morphological, polarization and spectral properties of different profile components. It received further support by calculations of the opening angles of different beams from the measurements of pulse widths (Rankin 1990; 1993 a, b; Gil, Kijak & Seiradakis 1993; Kramer 1994 and Kramer et al. 1994). According to Rankin's classification scheme (see below) different profile species correspond to different cuts through a nested multiconal pulsar beam. It is possible to distinguish the core component from the conal ones not only by its location within a pulse window (although generally the core component is flanked by one, two or even three pairs of conal components), but also by its different mean polarization and spectral characteristics as well as modulation properties of corresponding single pulses. The conal components usually show a relatively high degree of linear polarization with a regular swing of the mean position angle following the so-called Rotating Vector Model (RVM, Radhakrishnan & Cooke 1969), but typically weak circular polarization. The subpulses corresponding to conal components often show orderly subpulse drift or at least periodic intensity modulations. On the other hand, the subpulses in core components are rather longitude-stationary, i.e. they show no apparent subpulse drift or strong intensity modulation. The circular polarization in core components is quite high, often reversing sense at or near the phase of maximum intensity. The linear polarization position angle curve does not typically follow the RVM. Moreover, the spectra of core components are steeper than those of conal components, meaning that the former are more prominent at low radio frequencies while the latter dominate at higher frequencies.

By analyzing the above properties in a large number of pulsars Rankin (1983) distinguished seven major categories of pulse profiles: Multiple, Conal-triple, Quadruple, Triple, Conal-double, Conal-single and Core-single. We have marked different profile species by different colours in Fig. 6. One can immediately notice a tendency for grouping of different profile types in different regions of the $P-\dot{P}$ diagram. The separation seems to follow $P^{2.25}$ slope lines, corresponding to different values of the complexity parameter a , as suggested by equation (16). We will discuss this intriguing fact in the light of our spark-related, core/nested-conal model of the mean pulsar beam. We calculate the values of period derivative \dot{P}_{-15} from equation (16), using estimates of the parameter $a = 2n + 1$ based on the number of cones required in different profile categories, and then compare the results with the $P-\dot{P}$ diagram (Fig. 6) in which the complexity parameter a (represented by the size of the circles) is calculated from the equation (11), using only the basic pulsar parameters P and \dot{P} .

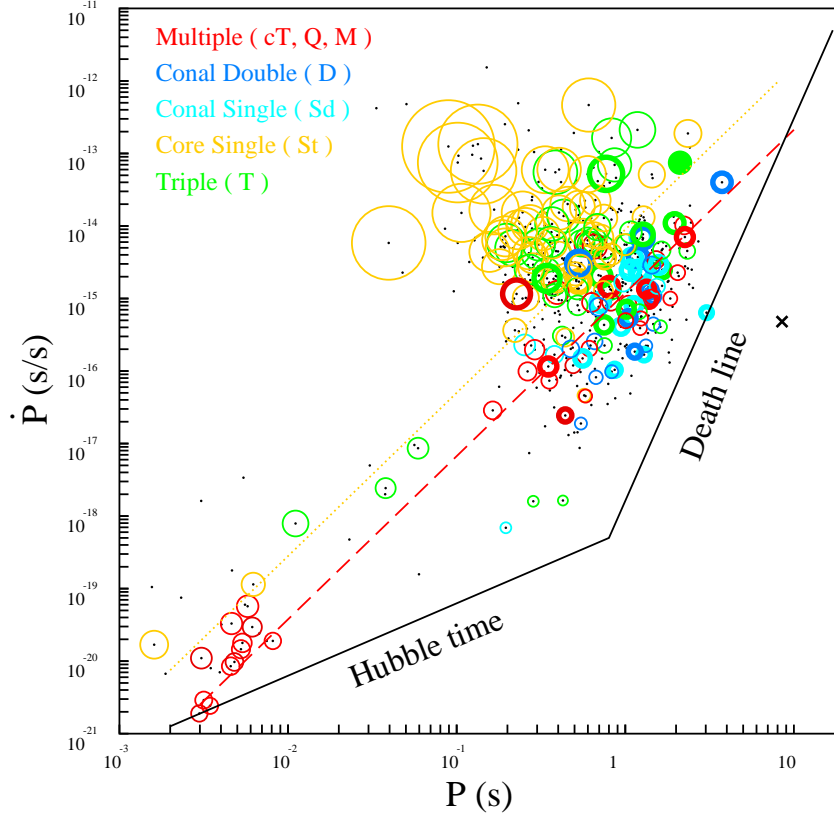


Fig. 6. | P - \dot{P} diagram for 539 pulsars with known (positive) period derivative (dots). In 182 pulsars for which pulse classification is established (see text) we mark by different size circles the values of the complexity parameter $a = r_p/h$ calculated from equation (11), and pulse class is marked by different colours. The values of a lie between about 1 (smallest circles) and 100 (largest circles) and we omit three youngest pulsars with $a > 100$ for scaling convenience. The number of sparks operating at any instant on the polar cap is approximately a^2 , that is from one spark in the right lower corner to about ten thousands in the left upper corner of diagram. The thicker circles indicate drifting subpulses and the green filled circle corresponds to the PSR 2002+31. The two lines with the $P^{2.25}$ slope (eq. [16] with $R_6 = 0.1$), correspond to $a = 5$ (multiple pulses - red) and $a = 10$ (lower limit for Core-single pulses - yellow), respectively. PSR J2144-3933 is marked by the cross. The Hubble time and conventional death line are also marked.

5.1. Multiple (red)

We will include in this class the Conal-triple (cT - three conal components), The Quadruple (Q - four conal components) and the Multiple (M - core component marked by two pairs of conal

components) profiles, since they all require $n = 2$ conal beam¹ corresponding to a $2n + 1 = 5$ (eq. [11]). The specific type of a profile depends on the observer's line-of-sight: M – cutting both the core and two conal beams, Q – cutting two cones but missing the core beam and cT – cutting the outer cone and grazing the inner cone.

Knowing the pulsar period and adopting the value of $a = 5$ for complex profile pulsars we can calculate the period derivative (eq. [16]) to within an accuracy determined by the range of R_6 and compare it with the measured value. For multiple profile pulsars the following relationship should hold $P_{15} \propto R_6 \dot{P}^{25}$. It seems that this is really so. In fact, the red dashed line in Fig. 6 corresponds to $R_6 = 0.1$ (see Appendix). Already Rankin (1992) has noticed that M-type pulsars with typical periods tend to follow a line with similar slope. Here we confirm this tendency for larger group of pulsars, including the millisecond ones.

5.2. Conal Double (dark blue) and Conal Single (light blue)

The Conal double profiles (D) have two conal components with no evidence of core emission in the saddle between them. While the D profiles are double in the entire pulsar spectrum, the Core single (S_d) profiles bifurcate only at low radio frequencies, clearly indicating that the observer is grazing the conal beam with the opening angle increasing as frequency decreases. In Conal Double profiles the observer's impact angle is smaller but in both cases the core beam is missing. In principle, one should consider one or two cones around the core beam, meaning that $n = 1$ or $n = 2$ and thus $a = 3$ or $a = 5$. Therefore, both D and S_d profile pulsars should occupy the common area with Multiple type pulsars. Figure 6 clearly shows that this is really so.

5.3. Core Single (yellow)

The Core single (S_t) profiles are simple (almost Gaussian) in shape, with prominent, sense-reversing circular polarization and rapid, non-RVM, position angle swings. No drifting subpulses have been found in S_t pulsars. More generally, the emission of S_t pulsars seems amorphous, with no hints of subpulse modulation in their single pulses. In principle, one has to consider two possibilities:

- (a) Just one (polar) spark with dimension comparable to the polar cap size. In such a case $r_p \approx h$, meaning that a mean-free path for B pair production is barely satisfied. It is no wonder then that S_t pulsars do not seem to occur in the region of small $a = 1$ in Fig. 6.

¹One can consider three or even four nested cones in exceptional cases (Gil & Kravczyk 1997, Kramer 1994, Gangadhara et al. 1999) but larger number of cones cannot be clearly resolved into profile components ($a > 10$, see section 5.3 for details). Evidence for a large number of, barely resolved, profile components is provided by Manchester et al. (1998) in their high resolution polarimetry of southern pulsars.

(b) A very large number of small sparks occupy the polar cap. This means that radiation of the adjacent sparks overlap and cannot be resolved into subpulses (components). Since the radiation is tangent to dipolar magnetic field lines to within an angle $1=\gamma$, where γ is the Lorentz factor of the emitting source, we have the condition $\gamma < 1=\gamma$. This implies that the difference of the opening angles² of field lines corresponding to adjacent sparks is smaller than the angular extent of elementary relativistic emission. For dipolar field lines, the opening angle $\approx 10^{-2} (d/r_p)^{1/2} (r/R)^{1/2} P^{-1/2}$, where $d < r_p$ is the distance from the pole to the base of the field line on the polar cap and $r = r_p = R$ is the emission altitude. Thus, $10^{-2} (D=r_p/r_p)^{1/2} P^{-1/2}$, where $D = d/h$ is a characteristic spark dimension and a typical distance between sparks. Kijak & Gil (1997, 1998) demonstrated that the emission altitude is apparently period dependent in such a way that $r_p^{1/2} P^{-1/2} \approx 10$. Since $D = r_p/h = 1/a$ (eqs. [9] and [12]), we have $a = 0.1/a < 1$ and if a is about 100 we conclude that $a > 10$ for the S_t profile pulsars. Thus, the Core Single pulsars should lie predominantly above the yellow dotted line in Fig. 6, corresponding to $a = 10$ calculated from equation (11).

The above consideration strongly suggests that the maximum number of nested cones (eq. [12]) that can be resolved as profile components is about 4. Interestingly, Mitra & Deshpande (1999) have recently found, on completely different grounds, that the number of nested cones within the overall pulsar beam is not larger than 4. Therefore, according to equations (12), (11) and (13), the number of resolved profile components should not exceed 9, which seems to be confirmed observationally. Few millisecond pulsars were reported to show more than 7 profile components (Kramer et al. 1998), which was a result of including complex interpulses, as well as pre- and post-cursors, in the component count. However, one cannot exclude even nine-component profiles for which $a = 9$, and such a case was recently reported by Gangadhara et al. 1999.

It is well known that about 65% of S_t profile pulsars develop weak conal outriders at high frequencies, where the core emission is no longer a dominant component of pulsar emission. We propose an explanation of this phenomenon which at first sight may seem a bit speculative, but a closer look shows that it can be quite plausible. The gap height h (which determines in our model both a spark dimension and a distance between sparks) depends on the magnetic field like $B^{4/7}$. In a multipolar surface magnetic field it can happen that the value of B drops by a factor of several to ten from the local pole to the polar cap edge. In such a case the side sparks would be a few times larger than the polar ones. If the condition $a = r_p/h > 0.1$ is not satisfied at the polar cap boundaries, the side sparks can form an outer cone of emission surrounding the core beam (resulting from unresolved emission of a large number of much smaller sparks well inside the polar cap). One cannot exclude that an undetectable outer beam always exists in the S_t profile pulsars and therefore the core emission of these objects represents only the inner part of the polar cap.

²The opening angle is an angle between the magnetic dipole axis (pulsar beam axis) and tangent to dipole field line corresponding to a particular emission feature.

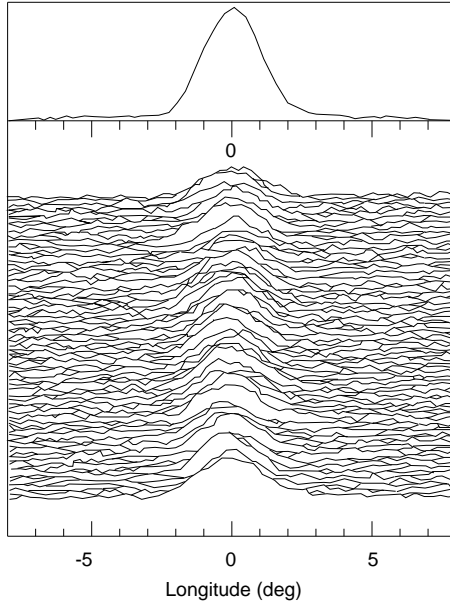


Fig. 7. | 430 MHz total intensity observational data of PSR B2002+31 taken at 430 MHz in the Arecibo Observatory. Note that both the mean profile (top) and individual pulses of this pulsar have similar Gaussian shapes. The position of PSR B2002+31 in Fig. 6 is marked by filled symbol.

5.4. Triple (green)

A genuine Triple (T) profile consists of a central core component flanked by a pair of conal outriders in the entire pulsar spectrum (although the core component may sometimes disappear at high frequencies). Here again we have two possibilities:

- (a) Just one cone around the core beam and an almost central line-of-sight trajectory. This case corresponds to $n = 1$ and $a = 3$ (eqs. [12] and [11]) and thus T profile pulsars should occupy a region on the P-P diagram corresponding to $a^{3.5} \approx 50$ in equation (16).
- (b) A large number of small sparks corresponding to $a > 10$, with the outer ring generated in the same way as in the case of the S_t profiles with outriders (section 5.3). The only difference is that the conal emission in T profile pulsars is not dominated by the core emission even at low frequencies, so they are of triple type in the entire pulsar radio spectrum. Since $a^{3.5} > 1000$ in equation (16), these pulsars should lie considerably above Multiple, Conal Double and Conal Single profile pulsars, overlapping partially with Core Single profile pulsars. This is really observed on the P-P diagram presented in Fig. 6.

A good example of T-prole pulsar with $a = 10$ is PSR B2002+31. This pulsar with $P = 2.11$ s and $P_{-15} = 75$ has the complexity parameter $a = 11$ and lies just above the yellow dotted line corresponding to $a = 10$ in Fig. 6 (filled green circle). The Gaussian waveform (Fig. 7) in the prole centre (top) consist of almost Gaussian individual pulses (each, in our interpretation, corresponding to a large number of "unresolved" sparks). The flat prole wings evolve into a pair of conal outriders at higher frequencies above 1 GHz (e.g. Gould & Lyne 1998, Table 4).

6. Discussion and Summary

There is a growing evidence from pulsars with orderly drifting subpulses (Deshpande & Rankin 1999; Vivekanand & Joshi 1999) that the RS75-type polar gap does exist (Xu et al. 1999). Analyzing observational properties of both single pulses and mean profiles we have found that the height scale of inner gap should be close to the value given by RS75. Although the physics behind our model is constrained only by dimensional analysis, it is a useful empirical base for more detailed modeling and interpretation of observations. We demonstrate that all periodicities associated with drifting subpulses are determined mainly by the P and P_{-} values. If the observing geometry is known, then one can even reproduce patterns of drifting subpulses. We found an amazing agreement between simulated and observed drift-bands in a number of cases (Table 1).

Throughout this paper we assume and/or argue that:

- (1) At any given time the polar cap is populated as densely as possible with a number of isolated spark discharges. This number is approximately equal to $a^2 \approx 25 P_{-15}^{0.6} P^{1.3}$.
- (2) A spark characteristic dimension as well as the typical distance between sparks is about the polar gap height $h \approx 3 \times 10^{1+7} P_{-15}^{2+7}$ cm.
- (3) The life-time (exponentiation time $\tau_R = c$) of each spark is of the order of 10 microseconds but they tend to reappear in almost the same places on time-scales shorter than $h = c \approx 10$ sec.
- (4) The actual surface magnetic field is dominated by multipole components. The planes of field lines tend to converge towards a local pole, which does not coincide in general with the global dipole axis. We believe that the actual surface magnetic field has a "sunspot-like" structure with one pole at the dipolar polar cap.
- (5) One spark is anchored quasi-permanently (oscillating on 10 s time scale) to the local pole, while other sparks perform a circumferential $E \times B$ drift around the polar spark.
- (6) Sparks supply a corresponding subpulse-associated plasma columns that can give rise to coherent radio emission due to some instability developing in a purely dipolar magnetospheric region at altitudes of about few percent of the light-cylinder radius $R_L = cP/2$.

- (7) The polar spark is associated with the core pulsar emission while other sparks circulate around the pole and contribute to the conal pulsar emission.

The assumptions and/or arguments used in this paper lead to nested-cones model of the mean pulsar beam. Such a beam structure has already been deduced by Rankin (1983) as a result of her profile classification scheme. This has been confirmed later by the analysis of the period dependence of pulse widths of different profile species (Rankin 1993 a,b; Gil, Kijak & Seiradakis 1993; Kramer et al. 1994; Gil & Krawczyk 1996, Gil & Han 1996, Mitra & Deshpande 1999). It is worth mentioning that our arguments are completely different from those of Rankin. Therefore, the fact that our model predictions are in excellent agreement with Rankin's classification scheme is not trivial.

The number of nested cones surrounding the core beam depends in our model mainly on basic pulsar parameters P and P_{-} (a dependence on the unknown parameters characterizing the structure of the actual surface magnetic field is rather weak). Therefore we can make three strong model predictions:

- (a) The Core Single (S_t) and Conal Single (S_d) profile pulsars should be well separated on the P ; P_{-} diagram (Fig. 6). A division line corresponds to a $\tau_p = 10$ (yellow dotted).
- (b) The single pulse emission in S_t pulsars (with $a > 10$) should be amorphous with no hints of modulation on the subpulse time scales, while S_d pulsars should demonstrate subpulses in their single pulses.
- (c) The subpulses in core components of complex profiles should be longitude-stationary while an apparent subpulse drift or periodic intensity modulation should occur exclusively in conal components.

These predictions, which seem to be supported observationally, are a direct consequence of a non-stationary polar gap discharge through a number of isolated sparks, reappearing in almost the same place for a long time as compared with their lifetime. This is an important advantage of sparking models over stationary free-flow models, where all the above observational features have no natural, self-consistent explanation. Perhaps an even more important advantage of a non-stationary polar gap discharge is the generation of a two-stream plasma instability in the magnetosphere near the neutron star (Usov 1987; Asseo & Melikidze 1998). The sparking phenomenon creates a succession of plasma clouds moving along magnetic field lines, each containing particles with a large spread of momenta. Overlapping of particles with different energies from successive clouds ignites strong Langmuir oscillations, which may lead eventually to the generation of coherent pulsar radio emission (Melikidze, Gil & Pataraya 1999). Interestingly, this instability is the only one which, according to our knowledge, develops at altitudes of the order of 1 percent of the light cylinder radius, where the pulsar radio emission is expected to originate (Cordes 1978, 1992; Kijak & Gil 1997, 1998). However, the latter statement is again true only if the potential drop height scale in the actual polar gap is close to that described by the RS75.

In the accompanying paper Melikidze, Gil & Pataraya (1999) examine a non-linear evolution of Langmuir electrostatic oscillations in plasma clouds associated with sparks reappearing at approximately the same place of the polar cap, according to a model presented in this paper. They found that a well known modulational instability leads to formation of a "bunch-like" charged solitons, capable of generating coherent curvature radiation at radio wavelengths. Thus, we believe that the non-stationary sparking discharge of the polar gap driven by non-dipolar surface magnetic field explains not only observational characteristics of pulsar radiation modulation but also the mysterious generation mechanism of this radiation, all in a self-consistent way.

Acknowledgements This paper is supported in part by the KBN Grant 2 P 03D 015 12 of the Polish State Committee for Scientific Research. We thank A. A. Deshpande, J. M. Rankin, M. Vivekanand and B. C. Joshi for providing us raw data with drifting subpulses. We also thank K. S. Cheng, T. H. Hankins, A. Krawczyk, G. Melikidze, D. Mitra and L. Nowakowski for their valuable contributions to this work. We thank F. C. Michel, D. Nice, B. Zhang and L. Zhang for helpful discussions and especially Z. Arzumanyan, M. Kramer and D. Lorimer for critical reading of parts of the manuscript and many useful comments. We also thank E. Gil for technical assistance. The Arecibo Observatory is operated by Cornell University under a Cooperative Agreement with the U.S. National Science Foundation.

A. Sunspot-like type surface magnetic field

Radio pulsars are believed to turn off when they can no longer produce electron-positron pairs in strong magnetic fields just above the polar cap. The limiting rotational period P_{at} at which this occurs depends on the magnitude and configuration of the surface magnetic field $B_s = b B_p$ (see eq. [6]). Unfortunately, only the perpendicular component of dipolar field B_d can be deduced from the observed spin-down rate \dot{P} , i.e. $B_d = 3.2 \cdot 10^8 (P \dot{P})^{1/2}$ Gauss. The line on the $B_d - P$ plane or $\dot{P} - P$ plane corresponding to the critical period is called a death line. No radio pulsar should be observed to the right of this line i.e. with period longer than the critical one. Recently, Young et al. (1999) reported the existence of PSR J2144-3933 with a period of 8.5 s, which is located to the right of all known death lines. As Young et al. (1999) conclude themselves, under the usual assumptions, this slowly rotating pulsar should not be emitting a radio beam.

Here we consider a death-line problem for PSR J2144-3933, assuming our preferred configuration of surface magnetic field, that is a sunspot type. Following Chen & Ruderman (1993) we can write the death-line equation in the form

$$\log B_d = 1.9 \log P - \log B_s + 0.6 \log R + 21; \quad (\text{A } 1)$$

where we introduced radius of curvature R of surface field lines as the unknown variable in their equation (9). Setting parameters of PSR J2144-3933 $P = 8.5$ s and $B_d = 2 \cdot 10^8$ G, we find that $B_s > 10^3$ G and $R < 10^6$ cm. In fact, for $R = 10^6$ cm the surface field $B_s = 10^{14.06}$ G,

which is greater than the critical magnetic field $B_q = 4.4 \times 10^8$ G above which the photon splitting phenomenon would quench the radio pulsar (Baring & Harding, 1998). The entire manifold of marginal death lines following from the above equation applied to PSR J2144-3933 is represented by the solid line in Fig. 8. All points $(B_s; R)$ lying on this line correspond to death lines (eq. [A1]) which pass through PSR J2144-3933 marked by cross in Fig. 6. As one can see, the inferred radius of curvature R for strong field $B_s = B_d$ is about 10^5 cm. We believe, that the existence of PSR J2144-3933 is at least consistent, if not implicative, with a sunspot-like surface magnetic field at pulsar polar cap.

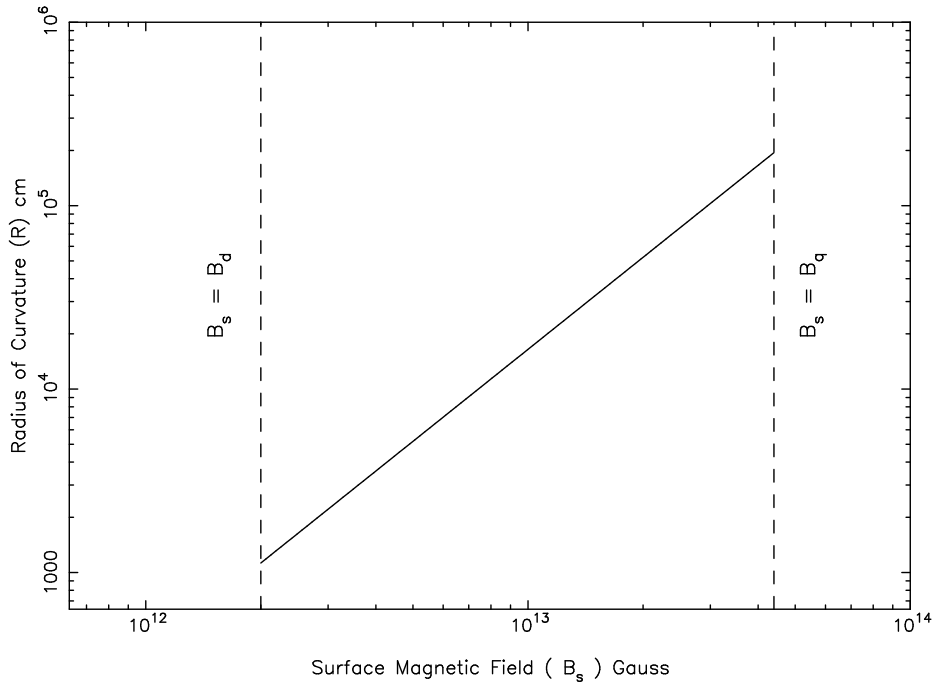


Fig. 8. | Radius of curvature R versus the magnitude B_s of the putative sunspot surface magnetic field in PSR J2144-3933 (eq. [A1] for $P = 8.5$ s and $B_d = 2 \times 10^8$ G). The two dashed vertical lines correspond to $B_s = B_d = 2 \times 10^8$ G and $B_s = B_q = 4.4 \times 10^8$ G, respectively. The position of PSR J2144-3933 in Fig. 6 is marked by the cross.

REFERENCES

- Arons, J., Sharlem an E . T . 1979, ApJ, 231, 854
- Arons, J. 1981, ApJ, 248, 1099
- Arons, J. 1993, ApJ, 408, 160
- Asseo, E ., Melikidze, G . 1998, MNRAS, 301, 59
- Baring, G . M ., Harding, A . K . 1998, ApJ, 507, L55
- Beskin, V . 1982, Soviet Astronomy, 26 (4), 443
- Blanford, R . D ., Applegate, J . H ., Hemquist L . 1983, MNRAS, 204, 1025
- Chen, K ., Rudern an, M . A . 1993, ApJ, 402, 264
- Cheng, A . F ., Rudern an, M . A . 1977, ApJ, 214, 598
- Cheng, A . F ., Rudern an, M . A . 1980, ApJ, 235, 576
- Cordes, J . M . 1978, ApJ, 222, 1006
- Cordes, J . M . 1992, Proc. of the IAU Colloq. 128, p 253, ed. Hanksins, T . H ., Rankin, J . M ., and G il J., Pedagogical University Press, Zielona G ora, Poland
- Deshpande, A . A ., Rankin, J . M . 1999, ApJ, 524, 1008
- Erber, T . 1966, Rev. Mod. Phy., 38, 626
- Filippenko, A . V ., Radhakrishnan V . 1982, ApJ, 263, 828
- Gangadhara, R . T ., Gupta, Y ., Lorimer, D . R . 1999, Proc. Pulsar Astronomy – 2000 and Beyond, ASP Conference Ser., M . Kram er, N . W ex and R . W iebinski, eds.
- G il, J., Hanksins, T . H ., Nowakowski, L ., 1992, Proc. of IAU Colloq. 128, p 133, ed. Hanksins, T . H ., Rankin, J . M ., and G il, J . A ., Pedagogical University Press, Zielona G ora, Poland, p 278
- G il, J., K ijak, J., Seiradakis, J . H . 1993, A & A , 272, 268
- G il, J., K ijak, J., Maron, O ., and Sendyk M . 1995, A & A , 301, 177
- G il, J., Krawczyk, A . 1996, MNRAS, 280, 143
- G il, J., Krawczyk, A . 1997, MNRAS, 285, 561
- G il, J., M itra, D . 1999, A & A , submitted
- Goldreich, P ., Julian, H . 1969, ApJ, 157, 869

- Gould, D. M. .1994, PhD Thesis, Manchester University
- Gould, D. M. ., Lyne, A. G. .1998, MNRAS, 301, 235
- Kijak, J., Gil, J. .1997, MNRAS, 288, 631
- Kijak, J., Gil, J. .1998, MNRAS, 299, 855
- Kramer, M. .1994, A & A Suppl. Ser., 107, 527
- Kramer, M. ., Wielebinski, R. ., Jessner, A. ., Gil, J. A. ., Seiradakis, J. H. .1994, A & A Suppl. Ser., 107, 515
- Kramer, M. ., Xiburis, K. M. , et al. 1998, ApJ, 501, 270
- Krolik, J. W. ., 1991, ApJ, 373, L69
- Lyne, A. G. . & Manchester, R. N. .1988, MNRAS, 234, 471
- Manchester, R. N. ., Johnston, S. .1995, ApJ, 441, L65
- Manchester, R. N. ., Han, J. L. ., Qiao, G. J. .1998, MNRAS, 295, 280
- Melickidze, G. I., Gil, J. & Pataraya A. D. .2000, ApJ, Paper II
- Mitra, D. ., Deshpande, A. A. .1999, A & A, 346, 906
- Mitra, D. ., Konar, S. ., Bhattacharya, D. .1999, MNRAS, 307, 459
- Radhakrishnan, V. ., Cooke, D. J. .1969, Astrophys. Lett., 3, 225
- Rankin, J. M. .1983, ApJ, 274, 333
- Rankin, J. M. .1986, ApJ, 301, 901
- Rankin, J. M. .1990, ApJ, 352, 314
- Rankin, J. M. .1992, Proc. of IAU Colloq. 128, p.133, ed. Hankins, T. H. ., Rankin, J. M. ., and Gil, J. A. ., Pedagogical University Press, Zielona Gora, Poland
- Rankin, J. M. .1993a, ApJ, 405, 285
- Rankin, J. M. .1993b, ApJ Suppl. Ser., 85, 145
- Romani, R. .1990, Nature, 347, 741
- Ruderman, M. A. ., Sutherland, P. G. .1975, ApJ, 196, 51 (RS75)
- Ruderman, M. A. .1991, ApJ, 366, 261 (RS)

- Sieber, W ., Oster, L . 1975, A & A , 38, 325
- Sharl~~em~~an, E . T ., Arons J., Faw ley W . M . 1978, ApJ, 222, 297
- Sturrock, P . A . 1971, ApJ, 164, 529
- Usov, V . V . 1987, ApJ, 320, 333
- Vivekanand, M ., Joshi, B . C . 1999, ApJ, 515, 398
- Xilouris, K M ., Kramer er, M ., Jessner, A ., von Hoensbroech, A ., Lorim er, D . R ., W ielebinski, R .,
W olszczan, A ., Cam ilo, F . 1998, ApJ, 501, 286
- Xu, R . X ., Q iao, G . J., Zhang, B . 1999, ApJ, 522, L109
- Young, M . D ., Manchester, R . N ., Johnston, S . 1999, Nature, 400, 848
- Zhang, B ., Q iao, G . J., Lin, W . P ., Han, J . L . 1997a, ApJ, 478, 313
- Zhang, B ., Q iao, G . J., Han, J . L . 1997b, ApJ, 491, 891
- Zhang, B . & Q iao, G . J . 1998, A & A , 338, 62

Table 1.

PSR B	P [s]	P_{-15}	a	n	N	$\frac{\hat{P}_3}{P}$	$\frac{P_3}{P}$	s_{out}	F	θ	ϕ
0943+10	1.09	3.52	6.8	3	20	37	1.85	0.875	0.125	26	8
2303+30	1.57	2.9	5	2	12	23	1.92	0.85	0.11	50	6.7
2319+60	2.26	7	5.2	2	9	70	7.8	0.85	0.12	27	3
0031-07	0.94	0.4	4	1	5	34	6.8	0.7	0.1	15	3.3

Note. | Pulsar name, period P , period derivative \dot{P} , in units of 10^{-15} s/s, complexity parameter a (eq. [11]), number of nested cones n (eq. [12]), number of circulating beams N within outermost cone, circulation period \hat{P}_3 (eq. [14]) in units of P , locus of the outermost cone s_{out} in units of the polar cap radius r_p , filling factor F (eq. [4]), inclination and impact (absolute value) angles in degrees.